

Constraining f_{NL} using the Large-Scale Modulation of Small-Scale Statistics

Utkarsh Giri¹* and Moritz Münchmeyer²

Department of Physics, University of Wisconsin-Madison, Madison, WI 53706, USA

Kendrick M. Smith²

Perimeter Institute for Theoretical Physics, Waterloo, ON N2L 3G1, Canada

(Dated: May 8, 2023)

We implement a novel formalism to constrain primordial non-Gaussianity of the local type from the large-scale modulation of the small-scale power spectrum. Our approach combines information about primordial non-Gaussianity contained in the squeezed bispectrum and the collapsed trispectrum of large-scale structure together in a computationally amenable and consistent way, while avoiding the need to model complicated covariances of higher N -point functions. This work generalizes our recent work, which used a neural network estimate of local power, to the more conventional local power spectrum statistics, and explores using both matter field and halo catalogues from the Quijote simulations. We find that higher N -point functions of the matter field can provide strong constraints on f_{NL} , but higher N -point functions of the halo field, at the halo density of Quijote, only marginally improve constraints from the two-point function.

I. INTRODUCTION

A main target of upcoming galaxy surveys of large-scale structure (LSS) like DESI [1], SPHEREx[?], EUCLID[2] and RUBIN OBSERVATORY[3] is to detect and characterize any non-Gaussianity in the primordial fields. Different models of inflation, as well as alternatives to inflation, predict primordial non-Gaussianity of various kinds which are sensitive to the field and energy content of the early universe [4, 5]. Among shapes of non-Gaussianity, the so called local type parameterized by f_{NL} ¹, which can detect multi-field inflation, is the most experimentally accessible with upcoming galaxy surveys. The primordial potential Φ under this parameterization is given by

$$\Phi(\mathbf{x}) = \Phi_G(\mathbf{x}) + f_{NL}(\Phi_G(\mathbf{x})^2 - \langle \Phi_G^2 \rangle) \quad (1)$$

where Φ_G is an auxiliary Gaussian field, and the phenomenological parameter f_{NL} controls the level of non-Gaussianity. Cosmic Microwave Background (CMB) experiments like Planck [6] have put strong constraints on f_{NL} using the bispectrum statistics of temperature and polarization maps. Further improvement is expected from LSS surveys in the coming years [7]. Although the lowest-order N -point statistic sensitive to f_{NL} in a weakly non-Gaussian universe is the bispectrum, the details of structure formation in an $f_{NL} \neq 0$ universe lead to *scale-dependent bias* in the power spectrum of density tracers like halos on the largest scales [8–10], making halo bias a promising and clean probe of f_{NL} in LSS. Its constraining power is expected to surpass the Planck CMB constraints in the very near future [11]. In

an $f_{NL} \neq 0$ universe, the halo power spectrum acquires a characteristic $1/k^2$ scaling that cannot be mimicked by any other physical process. However, the halo power spectrum is not the only statistic sensitive to f_{NL} , and attempts to develop new statistics are ongoing. Several recent works have tried to quantify the information gains one can hope to achieve from probing smaller scales. Approaches like field-level modelling [12], one-point analysis [13], and topological analysis [14], among others, have shown promise in extracting more information. In [15], we developed a neural network enhanced approach for constraining f_{NL} and obtained significantly better constraints on f_{NL} using information from the small-scale density field, while preserving the robustness of the scale-dependent bias analysis.

In this work, we go back to a more traditional approach and ask the question “how much f_{NL} information does the halo bispectrum add to the halo power spectrum?”. A number of recent papers have attempted to partially or completely answer this question [16–24].

There are several (related) challenges which must be addressed to answer this question. First, enumerating all nuisance parameters which must be marginalized is nontrivial, especially on quasilinear and smaller scales. One approach is the Effective Theory of LSS [25, 26]. Next, the observables (i.e. 2-point and 3-point functions) must be modelled in enough detail to marginalize nuisance parameters. Finally, it has been shown [20, 27, 28] that modelling the covariance between observables is critical. This is particularly challenging, since the covariance of (2+3)-point functions involves (4,5,6)-point functions which are difficult to compute.

Before explaining our approach, we will highlight two recent studies which are closely related to this paper. First, the Quijote-PNG collaboration [29–32] recently studied the f_{NL} information content of N -body simulations, by running enough simulations that the (2+3)-point observables and their covariance could be directly estimated from Monte Carlo. This approach is very flexi-

* Correspondence email address: ugiri@wisc.edu

¹ Throughout this work f_{NL} refers to local type primordial non-Gaussianity. We prefer it over the more common f_{NL}^{loc} parameterization for simplicity and conciseness.

ble, since it incorporates bispectrum information with arbitrary (k_1, k_2, k_3) dependence, and applies to any form of primordial non-Gaussianity, not just the local type considered in this paper. However, N -body simulations are computationally expensive, especially when pushed to scales where baryonic feedback is important [33–35]. Moreover, in a purely simulation-based approach it is difficult to marginalize a conservative set of nuisance parameters (such as EFT parameters). The Quijote-PNG analysis marginalizes Λ CDM cosmological parameters, and a minimum halo mass M_{\min} . With these caveats, the main result of [29–32] is that the 3-point function of the *matter* field contains significant f_{NL} information, but the 3-point function of the halo field does not (in the sense that $\sigma(f_{NL})$ in a (2+3)-point analysis is marginally better than a 2-point analysis).

Second, Goldstein et al [36] studied f_{NL} information in the matter bispectrum. The key idea of this paper is to restrict attention to the squeezed bispectrum², rather than using the full bispectrum. Then there are consistency relations [37–39] which show that in the squeezed limit $k_L \ll k_S$, the leading term in the bispectrum is proportional to (f_{NL}/k_L^2) . On the other hand, non-primordial physics produces contribution with a “softer” scale dependence $\mathcal{O}(k_L^0) + \mathcal{O}(k_L^2) + \dots$. By marginalizing a general contribution of this softer type, one automatically marginalizes all physical nuisance parameters (cosmological or astrophysical).

Our approach is similar in spirit to [36], but extended as follows. First, we will show that the squeezed bispectrum can be equivalently represented as a cross power spectrum $P_{\delta_m \pi}$, where the field $\pi(\mathbf{x})$ is the locally measured small-scale power spectrum (see Eq. 10 below for precise definition). Similarly, the collapsed trispectrum can be represented as the auto power spectrum $P_{\pi\pi}$ [20, 40].

We then argue heuristically (and verify with Quijote-PNG simulations) that on large scales, the field $\pi(\mathbf{x})$ is described by a linear bias model of schematic form (see Eq. 19 for precise form):

$$\pi(\mathbf{k}) \sim \left(b_\pi + \beta_\pi \frac{f_{NL}}{k^2} \right) \delta_m(\mathbf{k}) + (\text{white noise}) \quad (2)$$

Using this bias model, it is straightforward to write down a “field-level” likelihood function using large-scale modes of δ_m and π (Eq. 35 below), which captures f_{NL} information from the squeezed bispectrum ($P_{m\pi}$) and collapsed

trispectrum ($P_{\pi\pi}$). When we sample the likelihood, we marginalize all Gaussian bias parameters b_π (but not non-Gaussian biases β_π), and a set of parameters $N_{\pi\pi'}$ describing the white noise. We retain sensitivity to f_{NL} because the non-Gaussian signal in Eq. (2) has a characteristic $(1/k^2)$ scale dependence (like non-Gaussian halo bias or the squeezed bispectrum from [36]) which makes the analysis robust to uncertain cosmological and astrophysical parameters, without needing to enumerate these parameters explicitly.

The simplicity and low computational cost of our approach makes it easy for us to explore variants of the analysis – for example we study bispectra and trispectra of the halo field δ_h (rather than the matter field δ_m) in §V B. The basic idea of encoding higher-point information in the large-scale modes of an auxiliary π -field originated in [15], where we constructed a π -field using a convolutional neural network. A CNN can learn a π -field that gives optimal f_{NL} constraints and can thus improve over the locally measured small-scale power spectrum which we use here, at the cost of introducing a machine learning element.

We present our approach and develop an end-to-end mode based MCMC pipeline to explore the constraining power of the formalism. We analyze the matter field from the Quijote N -body simulation datasets [41] focusing particularly on the non-linear regime. We then analyze halo catalogues from the corresponding set of simulations. After presenting our formalism in II and III, in section IV, we present details of the Quijote simulation suite and our processing pipeline, which we use for validation and analysis. In section V, we present the results from our MCMC analysis. Finally in VI, we present our conclusions.

II. FORMALISM

In this section we will describe our approach intuitively with details postponed to subsequent sections. For conciseness, we present the formalism in terms of the halo overdensity field δ_h , but subsequent sections will generalize this to other cosmological fields (like the matter field δ_m).

Suppose we are interested in constraining f_{NL} using the squeezed halo bispectrum

$$\langle \delta_h(k_L) \delta_h(k_S) \delta_h(k'_S) \rangle \quad \text{where } k_L \ll k_S \quad (3)$$

and suppose we further assume that we average over a wide bin in k_S .

The squeezed bispectrum (3) can be viewed more intuitively as the cross power spectrum $P_{\delta_h \pi}(k_L)$, where $\pi(\mathbf{k}_L)$ is the locally observed small-scale halo power spectrum, integrated over a wide range of wavenumbers k_S . (For the formal definition of “locally observed small-scale power spectrum”, see §II B – here we just note that π is built quadratically out of small-scale modes of δ_h .)

² Recall that a three-point function (or bispectrum)

$$\langle \delta(\mathbf{k}_L) \delta(\mathbf{k}_S) \delta(\mathbf{k}_S') \rangle$$

is said to be *squeezed* if $k_L \ll \min(k_S, k'_S)$. A four-point (or trispectrum) configuration

$$\langle \delta(\mathbf{k}_1) \delta(\mathbf{k}_2) \delta(\mathbf{k}_3) \delta(\mathbf{k}_4) \rangle$$

is said to be *collapsed* if $|\mathbf{k}_1 + \mathbf{k}_2| \ll \min(k_1, k_2, k_3, k_4)$.

On large scales, the halo overdensity can famously be modelled as (schematically)

$$\delta_h(\mathbf{k}_L) = \left(b_h + \beta_h \frac{f_{NL}}{k_L^2} \right) \delta_m(\mathbf{k}_L) + \epsilon_h(\mathbf{k}_L) \quad (4)$$

where b_h and β_h are the usual Gaussian and non-Gaussian halo bias parameters respectively, while $\epsilon_h(\mathbf{k}_L)$ is the Poisson noise. We will argue that the new field $\pi(\mathbf{k}_L)$ can be modelled on large scales using a similar linear bias model:

$$\pi(\mathbf{k}_L) = \left(b_\pi + \beta_\pi \frac{f_{NL}}{k_L^2} \right) \delta_m(\mathbf{k}_L) + [\text{Noise } \epsilon_\pi(\mathbf{k}_L)] \quad (5)$$

where the power spectra of the noise fields ϵ_h , ϵ_π approach constants as $k \rightarrow 0$:

$$\begin{pmatrix} P_{\epsilon_h \epsilon_h}(k) & P_{\epsilon_h \epsilon_\pi}(k) \\ P_{\epsilon_h \epsilon_\pi}(k) & P_{\epsilon_\pi \epsilon_\pi}(k) \end{pmatrix} \rightarrow \begin{pmatrix} N_{hh} & N_{h\pi} \\ N_{h\pi} & N_{\pi\pi} \end{pmatrix} \text{ as } k \rightarrow 0 \quad (6)$$

These expressions involve some new parameters b_π , β_π , $N_{h\pi}$, and $N_{\pi\pi}$ (Note that $N_{hh} \approx 1/n_h$, where n_h is the halo number density). These new parameters would be difficult to calculate analytically (e.g. in the halo model) but we will describe a brute force procedure for estimating them from an ensemble of N -body simulations, in §IV C.

After all parameters in Eqs. (4)–(6) have been determined, we have a simple picture with two fields δ_h, π with f_{NL} -dependent power spectra. The original question, “how much f_{NL} information does the halo bispectrum add to the halo power spectrum?” can be rephrased as the question “how much f_{NL} information does $P_{h\pi}$ add to P_{hh} ?”.

We can also consider several generalizations of the approach as follows:

- In the two-field picture, one could also ask how much f_{NL} information can be obtained if $P_{\pi\pi}$ is included (in addition to $P_{hh}, P_{h\pi}$). In N -point language, this corresponds to asking how much f_{NL} information is obtained if the *collapsed* halo trispectrum is included (in addition to the halo power spectrum and squeezed bispectrum).
- So far, we have assumed for simplicity that the squeezed bispectrum is integrated over a wide range of small-scale wavenumbers k_S . This implicitly assumes a fixed k_S -weighting. To allow an arbitrary weighting, we could define a few k_S -bins, and define one π field for each bin. Then, instead of having two large-scale fields (h, π), we would have $(N+1)$ fields (h, π_i), where N is the number of k_S -bins. Similarly, we could allow an arbitrary halo mass weighting by defining multiple h and π fields corresponding to different halo mass bins.
- Instead of using the halo field δ_h , one could assume that the matter field δ_m can be observed on small

scales, to study the f_{NL} information limit for the true, noiseless matter field. (We will do this in §V A, before moving on to the halo case in §V B.)

- We could replace the locally measured small-scale power spectrum π (a quadratic function of δ_h) by a more complex nonlinear function. For example, one could use a convolutional neural network (CNN), or the wavelet scattering transform (WST) [42]. In [15], we constructed a nonlinear field $\pi(\mathbf{x})$ from small-scale modes of the matter field, using a CNN that was optimized for sensitivity to f_{NL} . In [43], an f_{NL} -optimized observable was constructed from galaxy catalogs (including color information) using machine learning methods.

In the following sections, we describe our formalism in detail.

A. Fourier conventions

Our Fourier conventions in a finite pixelized box, with box volume V_{box} and pixel volume V_{pix} , are:

$$\phi(\mathbf{x}) = V_{\text{box}}^{-1} \sum_{\mathbf{k}} \phi(\mathbf{k}) e^{i\mathbf{k}\cdot\mathbf{x}} \quad (7)$$

$$\phi(\mathbf{k}) = V_{\text{pix}} \sum_{\mathbf{x}} \phi(\mathbf{x}) e^{-i\mathbf{k}\cdot\mathbf{x}} \quad (8)$$

$$\langle \phi(\mathbf{k}) \psi(\mathbf{k}')^* \rangle = V_{\text{box}} P_{\phi\psi}(k) \delta_{\mathbf{k}\mathbf{k}'} \quad (9)$$

B. Observables

We define an *observable* of an N -body simulation to be a 3-d field $\pi(\mathbf{x})$ which is derived from the simulation, in a way which preserves the symmetries of the simulation volume (translations and permutations/reflections of the axes). Here are some examples of observables:

- The matter density field $\rho_m(\mathbf{x})$.
- The halo number density field $n_h(\mathbf{x})$, for some choice of halo mass bin (or halo mass weighting).
- The locally measured small-scale matter power spectrum

$$P_{mm}^{\text{loc}}(\mathbf{x}) = \left(\int \frac{d^3\mathbf{k}}{(2\pi)^3} W(k) \rho_m(\mathbf{k}) e^{i\mathbf{k}\cdot\mathbf{x}} \right)^2 \quad (10)$$

where $W(k)$ is a high-pass filter peaked at some characteristic small scale k_S . (The normalization of P_{mm}^{loc} in Eq. (10) is arbitrary.)

- Similarly, given a choice of halo mass bin (or halo mass weighting), we can define the locally measured small-scale halo power spectrum

$$P_{hh}^{\text{loc}}(\mathbf{x}) = \left(\int \frac{d^3\mathbf{k}}{(2\pi)^3} W(k) n_h(\mathbf{k}) e^{i\mathbf{k}\cdot\mathbf{x}} \right)^2 \quad (11)$$

C. Bias and noise

We now provide rigorous definitions for some central quantities used throughout this paper. In particular, we define the Gaussian bias (b_π), the non-Gaussian bias (β_π) as well as the noise $N_{\pi\pi'}$ for an observable π described in the last section.

The large-scale (Gaussian) *bias* b_π is defined by:

$$\lim_{k \rightarrow 0} P_{\pi\delta_m}(k) = b_\pi P_{mm}(k) \quad (12)$$

Another way of thinking about bias is:

$$\pi(\mathbf{k}) = b_\pi \delta_m(\mathbf{k}) + (\text{Noise field } \epsilon_\pi(\mathbf{k})) \quad (13)$$

where the noise field ϵ_π defined by this equation is uncorrelated with δ_m on large scales. In the special case where $\pi = n_h$ is the halo number density field, then $b_\pi = \bar{n}_h b_h$, where b_h is the usual halo bias.

For a pair of observables π, π' , we define the *noise* $N_{\pi\pi'}$ by:

$$\lim_{k \rightarrow 0} P_{\pi\pi'}(k) = b_\pi b_{\pi'} P_{mm}(k) + N_{\pi\pi'} \quad (14)$$

If observables π_1, \dots, π_n are halo number density fields $\pi_i = n_{h_i}$ corresponding to different mass bins, then $N_{\pi_i\pi_j} = \bar{n}_{h_i} \delta_{ij}$. This statement assumes a Poisson noise model for halos.

Finally, we define the *non-Gaussian bias* β_π by:³

$$\beta_\pi \equiv \frac{\partial \bar{\pi}}{\partial \log \sigma_8} \quad (15)$$

where the quantity $\bar{\pi}$ is the mean value of $\pi(\mathbf{x})$, taken over both Monte Carlo simulations and spatial pixels.

If $\pi = n_h$ is the halo number density field, then the non-Gaussian bias β_π is given by the famous equation (with an extra factor \bar{n}_h since we use $\pi = n_h$ instead of $\pi = \delta_h$):

$$\beta_\pi \approx \bar{n}_h \delta_c (b_g - 1) \quad (16)$$

where $\delta_c \approx 1.42$. This is really an approximation to the true non-Gaussian bias $\beta_h \equiv (\partial \bar{n}_h / \partial \log \sigma_8)$. The approximation in Eq. (16) is motivated by spherical collapse models of halo formation, and is usually accurate to $\sim 10\%$ when compared with simulations [44, 45].

The non-Gaussian bias β_π parametrizes the level of excess clustering on large scales in an f_{NL} cosmology, in a sense that we will make precise in the next section.

III. f_{NL} COSMOLOGY

A. Key conjectures

In the previous section, we defined the bias b_π and noise $N_{\pi\pi'}$ by the the large-scale ($k \rightarrow 0$) power spectra:

$$P_{g\pi}(k) \rightarrow b_\pi P_{mm}(k) \quad (17)$$

$$P_{\pi\pi'}(k) \rightarrow b_\pi b_{\pi'} P_{mm}(k) + N_{\pi\pi'} \quad (18)$$

So far, we have assumed $f_{NL} = 0$. In this section, we will generalize Eqs. (17), (18) to an f_{NL} cosmology. We will describe these results as “conjectures”, to emphasize that they are predictions that we will verify with simulations later (§IV).

Key conjecture 1. In an f_{NL} cosmology, Eq. (17) generalizes as (on large scales):

$$P_{m\pi}(k) = \left(b_\pi + 2\beta_\pi \frac{f_{NL}}{\alpha(k, z)} \right) P_{mm}(k) \quad (19)$$

where β_π was defined in Eq. (15). The function $\alpha(k, z)$ is defined by:

$$\alpha(k, z) \equiv \frac{2k^2 T(k) D(z)}{3\Omega_m H_0^2} \quad (20)$$

so that $\delta_m(k, z) = \alpha(k, z) \Phi(k)$, where $\Phi(k)$ is the primordial potential from Eq. 1.

Note that $\alpha(k, z) \propto k^2$ as $k \rightarrow 0$, so the key conjecture (19) predicts that any observable with $\beta_\pi \neq 0$ has large-scale bias proportional to (f_{NL}/k^2) . This generalizes the famous non-Gaussian halo bias in the case $\pi = \rho_h$.

Key conjecture 2. In an f_{NL} cosmology, Eq. (18) generalizes as (on large scales):

$$P_{\pi\pi'}(k) = \left(b_\pi + 2\beta_\pi \frac{f_{NL}}{\alpha(k, z)} \right) \times \left(b_{\pi'} + 2\beta_{\pi'} \frac{f_{NL}}{\alpha(k, z)} \right) P_{mm}(k) + N_{\pi\pi'} \quad (21)$$

That is, the large-scale cross spectrum $P_{\pi\pi'}(k)$ has the “minimal” form expected from the bias model (19), plus a white noise term $N_{\pi\pi'}$.

Key conjecture 3. Given N observables π_1, \dots, π_N , the matter field $\delta_m(\mathbf{k})$ and the observables $\pi_i(\mathbf{k})$ are Gaussian fields for sufficiently small k . Thus, the higher point statistics and likelihood function of the field realizations are determined by the power spectra in key conjectures 1 and 2.

B. Schematic derivation of key conjectures 1 and 2

In an f_{NL} cosmology, the initial conditions are given by:

$$\Phi(\mathbf{x}) = \Phi_G(\mathbf{x}) + f_{NL}(\Phi_G(\mathbf{x})^2 - \langle \Phi_G^2 \rangle) \quad (22)$$

³ When we write $(\partial/\partial \log \sigma_8)$, we really mean a derivative $(\partial/\partial \log \Delta_c)$ with respect to the overall amplitude of the initial adiabatic curvature power spectrum $P_\zeta(k) = 2\pi \Delta_c^2 (k/k_{\text{piv}})^{n_s-4}$.

To analyze the effect of a long-wavelength mode, let us decompose the *Gaussian* potential as a sum $\Phi_G = \Phi_l + \Phi_s$ of long-wavelength and short-wavelength contributions. The long/short-wavelength decomposition of the non-Gaussian potential Φ is then

$$\begin{aligned} \Phi(\mathbf{x}) = & \underbrace{\Phi_l(\mathbf{x}) + f_{NL}(\Phi_l(\mathbf{x})^2 - \langle \Phi_l^2 \rangle)}_{\text{long}} \\ & + \underbrace{(1 + 2f_{NL}\Phi_l(\mathbf{x}))\Phi_s(\mathbf{x}) + f_{NL}(\Phi_s(\mathbf{x})^2 - \langle \Phi_s^2 \rangle)}_{\text{short}} \end{aligned} \quad (23)$$

and contains explicit coupling between long and short wavelength modes of the Gaussian potential.

The term $(1 + 2f_{NL}\Phi_l(\mathbf{x}))\Phi_s(\mathbf{x})$ in Eq. (23) may be interpreted as follows. In a local region where the long-wavelength potential takes some value Φ_l , the overall amplitude of the small-scale modes is multiplied by a factor $(1 + 2f_{NL}\Phi_l)$. That is, the ‘‘locally observed’’ value of σ_8 fluctuates throughout the universe, and is given on large scales by:

$$\sigma_8^{\text{loc}}(\mathbf{x}) = (1 + 2f_{NL}\Phi_l(\mathbf{x}))\bar{\sigma}_8 \quad (24)$$

These large-scale variations in σ_8 induce large-scale variations in the observable π as follows:

$$\pi(\mathbf{x}) = b_\pi \delta_m(\mathbf{x}) + \beta_\pi \log\left(\frac{\sigma_8^{\text{loc}}(\mathbf{x})}{\bar{\sigma}_8}\right) + (\text{uncorrelated noise}) \quad (25)$$

Here, the first and third terms arise in an $f_{NL} = 0$ cosmology. The second term is new, and arises because a fluctuation ($\delta \log \sigma_8^{\text{loc}}$) of sufficiently long wavelength has the same effect on the observable π as a shift ($\delta \log \sigma_8$) in the ‘‘background’’ cosmological parameter σ_8 .

Combining Eqs. (24), (25) and writing $\delta_m(k, z) = \alpha(k, z)\Phi(k)$, we obtain the following expression for $\pi(\mathbf{x})$ on large scales:

$$\pi(\mathbf{k}) = \left(b_\pi + 2\beta_\pi \frac{f_{NL}}{\alpha(k, z)}\right) \delta_m(\mathbf{k}) + (\text{uncorrelated noise}) \quad (26)$$

If we cross-correlate Eq. (26) with δ_m , the noise term goes away, and we get:

$$P_{m\pi}(k) = \left(b_\pi + 2\beta_\pi \frac{f_{NL}}{\alpha(k, z)}\right) P_{mm}(k) \quad (27)$$

which is key conjecture 1. If we cross-correlate the expression for $\pi(\mathbf{k})$ in Eq. (26) with a similar expression for a different observable $\pi'(\mathbf{k})$, we get:

$$\begin{aligned} P_{\pi\pi'}(k) = & \left(b_\pi + 2\beta_\pi \frac{f_{NL}}{\alpha(k, z)}\right) \\ & \times \left(b_{\pi'} + 2\beta_{\pi'} \frac{f_{NL}}{\alpha(k, z)}\right) P_{mm}(k) + N_{\pi\pi'} \end{aligned} \quad (28)$$

which is key conjecture 2. We validate both these conjectures using N -body simulations in the next section. In

the linear regime, the noise $N_{\pi\pi'}$ would be inversely proportional to the number of local modes per unit volume, while in the non-linear regime we use here, it is a more complicated function.

IV. SIMULATION PIPELINE

A. Simulations

A major challenge in simulation-based studies for constraining f_{NL} is the need for large sets of large-scale cosmological simulations with sufficiently high resolution, ideally run with both Gaussian as well as non-Gaussian initial conditions. Several collaborative efforts have been made recently to release massive suites of simulations, including both hydrodynamical and dark matter only simulations, for broad public use. In this paper, we utilize the Quijote suite of simulations [41], which consists of 44,100 publicly accessible, full N -body simulations that cover over 7,000 cosmological models within the cosmological parameter hyperplane, with varying particle resolution. These simulations are run using the Gadget-III [46] simulation code.

One of the primary aims of the Quijote simulations is to quantify information content on cosmological observables and as such, there are sets of simulations where a single parameter is perturbed above or below its fiducial value to facilitate numerical derivative computations using finite difference. In our work, we will be using the **fiducial** simulations to test our formalism along with the datasets **s8_m** and **s8_p** which we use to estimate non-Gaussian bias β (see Eq. (31) below). The **fiducial** simulations use $\Omega_m = 0.3175$, $\Omega_b = 0.049$, $h = 0.6711$, $n_s = 0.9624$, $w = -1$ and $\sigma_8 = 0.834$ and are run in a box of size $1 (h^{-1}\text{Gpc})^3$ using 512³ dark-matter particles to sample the matter field. The initial particle positions and velocities are generated using second-order Lagrangian perturbation theory [47] at redshift $z = 127$ and with a Gaussian primordial potential with an effective $f_{NL} = 0$. For the **s8_m** simulations, the σ_8 is lowered to 0.819 while **s8_p** simulations have $\sigma_8 = 0.849$. For all these simulations, the halo catalogue is generated using the classical Friends-of-Friend (FoF) algorithm [48] with a minimum particle requirement of 20 and a linking length of 0.2. To test our formalism for f_{NL} universe, we make use of Quijote-PNG simulations [31]. The Quijote-PNG are another large suite of N -body simulations which extend the Quijote simulations to include simulations with different types of primordial non-Gaussianity. They are run with PNG of local, equilateral and orthogonal type, each characterized by the parameter f_{NL} , with other cosmological parameters and simulation specifications kept identical to the fiducial Quijote simulations. There are two subsets, **LC_p** and **LC_m** which have local PNG with f_{NL} set to 100 and -100 respectively. In this study we make use of the **LC_p** suite.

B. Generating the π fields from density fields

For our study with Quijote simulations, we choose to work with simulations at $z = 0$. We use the public library `Pylians3` [49] to read binary snapshot files and use the cloud-in-cell algorithm [50] implemented in `nbodykit` [51] to paint particle positions on a 3D mesh to obtain the matter field ρ_m . We similarly paint the positions of the halos to obtain the halo number density field ρ_h . For both matter and halo field, our 3D mesh grid is of size 1024^3 . This choice of mesh size corresponds to Nyquist frequency $3.2 h \text{ Mpc}^{-1}$. This allows us to tap information from the deeply non-linear regime. The process of painting particle positions on a 3D mesh is known to suffer from an effect called ‘‘aliasing’’ which can potentially contaminate modes near the Nyquist frequency. Sampling and resolution related issues also become pronounced on small scales. However, we will show in §IV D that our key conjectures from §III A are still valid if we construct π -fields from wavenumbers near the Nyquist frequency.

We now define 5 matter-derived fields $\{\pi_i^m\}_{i=1,2,3,4,5}$, and 2 halo-derived fields $\{\pi_i^h\}_{i=1,2}$, which will be used extensively throughout the paper. Each such π -field is defined by:

$$\pi_i^f(\mathbf{x}) = \left(\int \frac{d^3\mathbf{k}}{(2\pi)^3} W^i(\mathbf{k}) \rho_f(\mathbf{k}) e^{i\mathbf{k}\cdot\mathbf{x}} \right)^2 \quad (29)$$

where $f \in \{m, h\}$ and $W^i(\mathbf{k})$ is a band-pass filter given by:

$$W^i(\mathbf{k}) = \begin{cases} 1 & \text{if } k_{\min}^i < |\mathbf{k}| < k_{\max}^i \\ 0 & \text{elsewhere} \end{cases} \quad (30)$$

As explained near Eqs. (10), (11) above, each such π -field corresponds intuitively to the locally measured small-scale power (in either the matter or halo field) in a certain k -range (k_{\min}^i, k_{\max}^i) .

For the 5 matter-derived fields π_i^m , we use the k -bins $(k_{\min}^i, k_{\max}^i) = \{(0.5, 1.0), (1.0, 1.5), (1.5, 2.0), (2.0, 2.5), (2.5, 3.0)\} h^{-1} \text{ Mpc}$. For the 2 halo-derived fields π_i^h , we use k -bins $(k_{\min}^i, k_{\max}^i) = \{(0.5, 1.0), (1.0, 1.5)\} h^{-1} \text{ Mpc}$.

C. Estimating bias and noise from simulations

In this section, we describe our procedure for estimating the parameters b_π , β_π , and $N_{\pi\pi'}$ from N -body simulations.

The simplest case is the non-Gaussian bias $\beta_\pi = \partial\bar{\pi}/(\partial\log\sigma_8)$. This is conceptually straightforward: we run two ensembles of simulations with different values σ_8^+ , σ_8^- of the cosmological parameter σ_8 . For each simulation s and choice of σ_8^\pm , we spatially average $\pi(\mathbf{x})$ to obtain a per-simulation mean $\bar{\pi}_s(\sigma_8^\pm)$. We then estimate $\beta_\pi = \partial\bar{\pi}/(\partial\log\sigma_8)$ by numerically differencing:

$$\hat{\beta}_\pi \equiv \frac{1}{N_{\text{sim}}} \sum_{s=1}^{N_{\text{sim}}} \frac{\bar{\pi}_s(\sigma_8^+) - \bar{\pi}_s(\sigma_8^-)}{\log(\sigma_8^+) - \log(\sigma_8^-)} \quad (31)$$

In our study, we use `s8_m` and `s8_p` suite of simulations produced by the Quijote collaboration and described in detail in IV to estimate β_π . The `s8_m` and `s8_p` simulations are run in pairs, with the same RNG seed and $\sigma_8^- = 0.819$ and $\sigma_8^+ = 0.849$ respectively. Thus we can estimate β_π by finite difference (Eq. (31)) around the fiducial simulation suite with $\sigma_8 = 0.834$.

Next, we discuss the Gaussian bias b_π and the noise $N_{\pi\pi'}$. These parameters are defined by the large-scale power spectra:

$$\begin{aligned} P_{m\pi}(k) &= b_\pi P_{mm}(k) \\ P_{\pi\pi'}(k) &= b_\pi b_{\pi'} P_{mm}(k) + N_{\pi\pi'} \end{aligned} \quad (32)$$

We fit for these parameters directly from simulation, using a mode-based likelihood similar to §VII in [15, 52]. We sketch the construction as follows. Given N observables π_1, \dots, π_N , we define the $(N+1)$ -component vector:

$$\theta(\mathbf{k}) = \begin{pmatrix} \delta_m(\mathbf{k}) \\ \pi_1(\mathbf{k}) \\ \vdots \\ \pi_N(\mathbf{k}) \end{pmatrix} \quad (33)$$

We also define the $(N+1)$ by $(N+1)$ covariance matrix $C(k)$ by:

$$\langle \theta(\mathbf{k}) \theta(\mathbf{k}')^\dagger \rangle = C(k) (2\pi)^3 \delta^3(\mathbf{k} - \mathbf{k}') \quad (34)$$

The matrix elements of $C(k)$ are given by Eq. (32), and depend on the parameters b_π , $N_{\pi\pi'}$. The model likelihood is given by:

$$\mathcal{L}(\Theta|\mathcal{D}) \propto \prod_k \frac{1}{\sqrt{\text{Det } C(k)}} \exp\left(-\frac{\mathcal{D}(\mathbf{k})^\dagger C(k)^{-1} \mathcal{D}(\mathbf{k})}{2V}\right)$$

which we sample using MCMC sampling code `emcee`[53] using conservative priors on model parameters $(b_\pi, N_{\pi\pi'})$. When additionally constraining f_{NL} in later sections, we use this same likelihood, with the covariance $C(k)$ generalized to include f_{NL} dependence using Eq. (19) and Eq. (21).

D. Validation on f_{NL} simulations

In this section we analyze N -body simulations with $f_{NL} \neq 0$. Our goal is to validate the key conjectures laid out in §III A, which predict clustering observables $P_{m\pi(k)}$ and $P_{\pi\pi'}(k)$ in a non-Gaussian cosmology. Throughout this section, we take the π fields to be the 5 matter-derived fields $\{\pi_i^m\}_{1 \leq i \leq 5}$ described in §IV B.

In the top panels of Fig. 1, we present the empirical bias $b_{\pi_i^m} = P_{m\pi_i^m}(k)/P_{mm}(k)$ from 50 simulations with $f_{NL} = 50$. The $1/k^2$ behaviour of the bias at the largest-scale is qualitatively evident. We also observe the bias

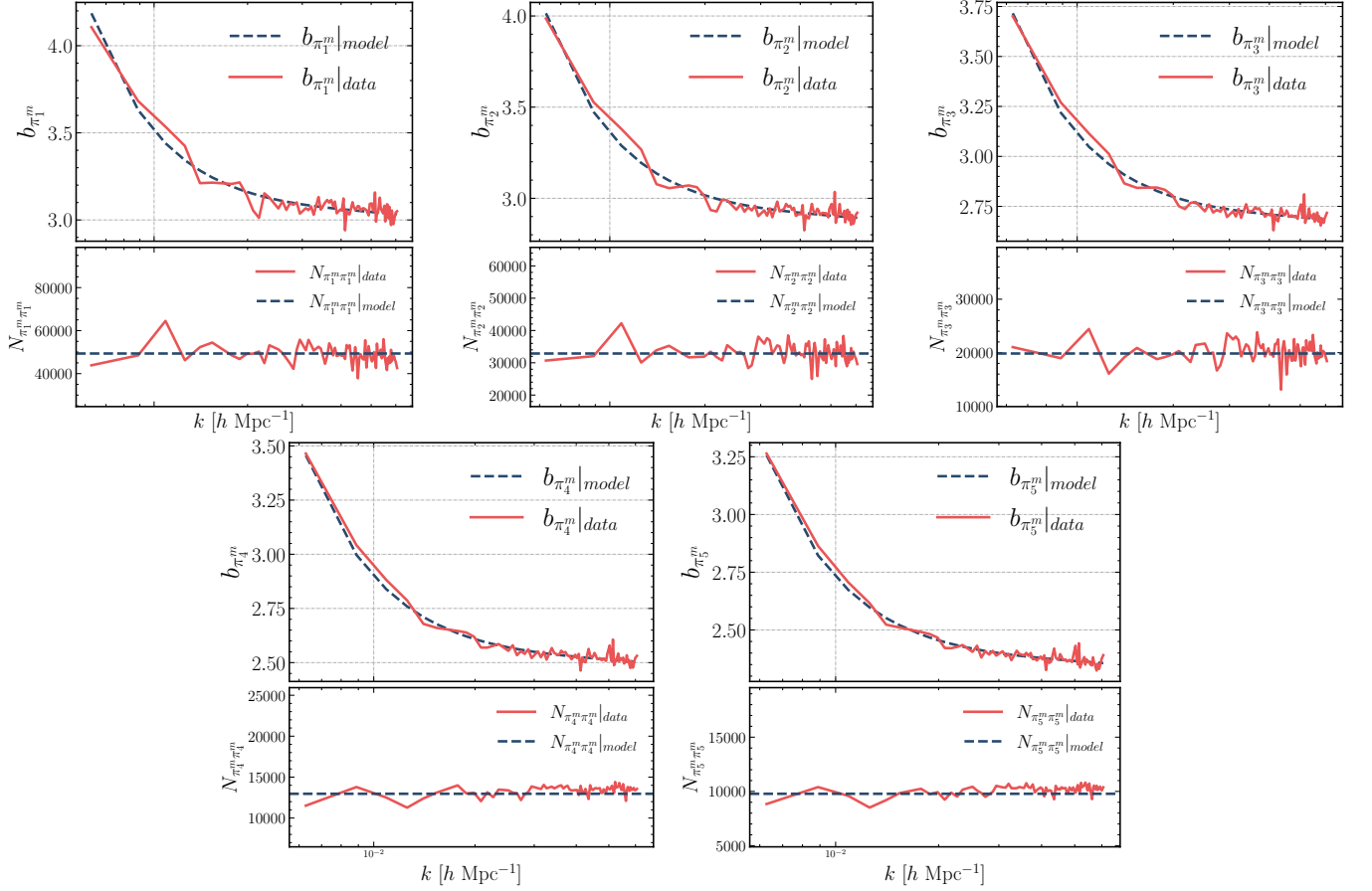


Figure 1. *Top panel.* Bias model (19) for the five matter-derived π fields $\{\pi_i^m\}_{1 \leq i \leq 5}$ defined in IV B compared to their empirical bias $b_{\pi_i^m} = P_{m\pi_i^m}(k)/P_{mm}(k)$ from simulations, for $f_{NL} = 100$. The best-fit model parameters ($b_{\pi_i^m}, N_{\pi_i^m}$) are obtained from the MCMC pipeline with $k_{\max} = 0.047$ h Mpc $^{-1}$. The agreement between the simulations and the model is excellent. *Bottom panel.* Noise power spectra $N_{\pi_i^m \pi_i^m}(k)$ for the π -fields, computed as described in §IV D, showing that the noise power spectrum is constant on large scales.

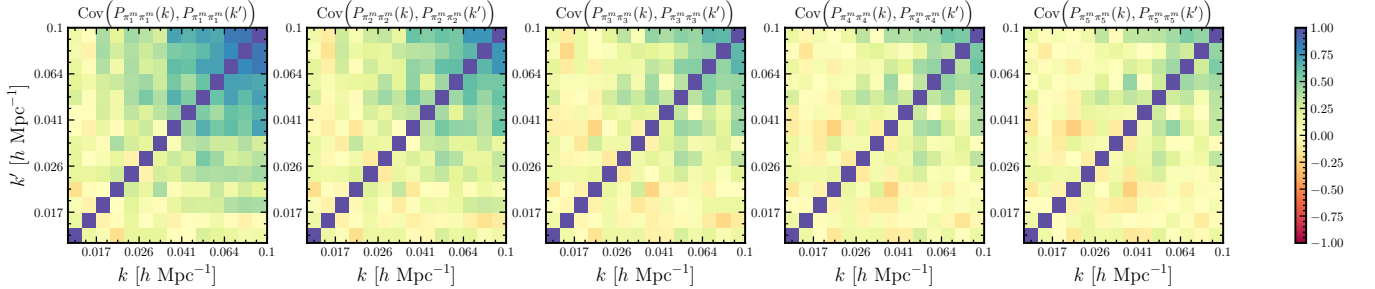


Figure 2. Power spectrum covariance $\text{Cov}(P_{\pi_i^m \pi_i^m}(k), P_{\pi_j^m \pi_j^m}(k'))$ for the matter-derived π -fields. The off-diagonal ($k \neq k'$) covariance is small on large scales. The covariance is estimated using 50 fiducial Quijote simulations.

approaching a constant value at $k \sim 0.1$ h $^{-1}$ Mpc. For a quantitative comparison, we also show model curves of the form $b(k) = b_{\pi} + 2\beta_{\pi}f_{NL}/\alpha(k, z)$. Here, the constant bias b_{π} is the best-fit value from an MCMC analysis, but the non-Gaussian bias β_{π} is estimated from σ_8^{\pm} simulations using Eq. (31).

In the bottom panels of Fig. 1, we present the noise

$N_{\pi_i^m \pi_i^m}$ for the π_i^m fields. To calculate the noise, we use Gaussian Quijote simulations with $f_{NL} = 0$. The noise is estimated by computing the power spectrum of the residual field defined by $\epsilon_i(\mathbf{k}) = \pi_i^m(k) - b_{\pi_i^m}(k)\delta_m(k)$ where $b_{\pi_i^m}$ is obtained using Eq. 12. As can be seen, the power spectrum of residual field agrees well with the noise obtained from an MCMC fit. These results conclude our

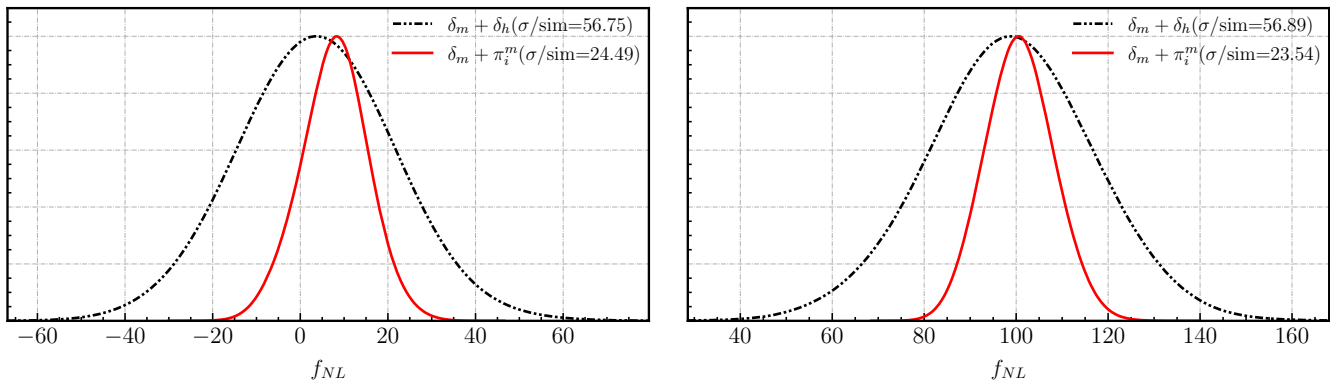


Figure 3. *Left.* MCMC constraints on f_{NL} from $\delta_m + \delta_h$ and $\delta_m + \pi_i^m$, using 10 Quijote **fiducial** simulations with Gaussian initial conditions ($f_{NL}=0$). The notation π_i^m refers to the combination of five π^m fields defined in IV B. These five fields correspond intuitively to locally measured small-scale matter power in five different k_S -bins. We find that an analysis with the fields $\delta_m + \pi_i^m$ (red color) improves error on f_{NL} by a factor 2.2 compared to a standard $\delta_m + \delta_h$ analysis (black curve). We use modes up to $k_{\max} = 0.047 h^{-1}\text{Mpc}$ corresponding to the largest 999 modes in the simulation volume. *Right.* Results from analysis of 10 Quijote-PNG **LC_p** simulations with $f_{NL} = 100$. The “ σ/sim ” value in the label denotes scaled uncertainty on f_{NL} obtained from a single simulation of volume 1 ($h^{-1}\text{Gpc}$)³.

validation of key conjectures 1 and 2 from §III A.

Our key conjecture 3 posits that on very large scales, the π fields are Gaussian. As evidence for this conjecture, in Fig. 2 we show the bandpower covariance $\text{Cov}(P_\pi(k), P_\pi(k'))$ estimated from N -body simulations. For $k \lesssim 0.05 h^{-1}\text{Mpc}$, the off-diagonals $k \neq k'$ are close to zero, as would be expected for a statistically homogeneous Gaussian field.

V. RESULTS

In this section, we consider the central question of this paper: do the squeezed 3-point and collapsed 4-point functions add f_{NL} information to a matter or halo power spectrum analysis?

In §V A, we will answer this question assuming that the matter field δ_m can be directly observed on large scales. In V B, we will assume that only the halo field is observed.

A. Matter field based results from Quijote

In our matter-based analysis, we constrain f_{NL} using large-scale power spectra of the form $P_{m\pi^m}(k)$ and $P_{\pi_i^m\pi_j^m}(k)$. Here, the fields $\{\pi_i^m\}_{1 \leq i \leq 5}$ were defined in §IV B, and correspond to locally measured small-scale matter power in a certain k -range (k_{\min}^i, k_{\max}^i). In traditional bispectrum language, the observables $P_{m\pi_i^m}(k)$ and $P_{\pi_i^m\pi_j^m}(k)$ correspond respectively to the squeezed matter bispectrum B_{mmm} and collapsed matter trispectrum T_{mmmm} .

In the left panel of Fig. 3, we present constraints on f_{NL} from an MCMC analysis which combines δ_m with

the π_i^m fields, using the mode-based likelihood defined in §IV C. The analysis combines 10 fiducial Quijote simulations with Gaussian initial conditions ($f_{NL} = 0$). We truncate the sum in Eq. 35 at a conservative $k_{\max} \sim 0.047 h^{-1}\text{Mpc}$ corresponding to the largest 999 modes of the simulation volume.

To describe the MCMC in more detail, we denote the six fields ($\delta_m(\mathbf{k}), \pi_i^m(\mathbf{k})$) by a six-component vector $\theta_i(\mathbf{k})$ as in Eq. (33). The 6×6 covariance $C(k)$ depends on f_{NL} , the Gaussian biases b_i , non-Gaussian biases β_i , and noise parameters N_{ij} (26 parameters total, accounting for the symmetry $N_{ij} = N_{ji}$). We pre-evaluate the non-Gaussian biases β_i by estimating their values in σ_8^\pm simulations (see Eq. (31)), and vary the parameters (f_{NL}, b_i, N_{ij}) in the MCMC. The pre-evaluation is done using 20 pairs of simulations and the estimated biases are $(\beta_h, \beta_1, \beta_2, \beta_3, \beta_4, \beta_5) = (0.589, 3.004, 2.924, 2.688, 2.483, 2.347)$. The statistical scatter in these values is $\sim 1\%$.

In the left panel of Fig. 3, we also show f_{NL} constraints from a more traditional analysis combining δ_m and δ_h . We find that the $(\delta_m + \pi^m)$ -based analysis gives a constraint on f_{NL} which is 2.2 times better than a $\delta_m + \delta_h$ analysis done for the same fiducial simulation volume. That is, the squeezed matter bispectrum is adding significant f_{NL} information.

In the right panel of Fig. 3 we present results from an analysis done using 10 **LC_p** simulations from Quijote-PNG simulation suite which have non-Gaussian initial conditions. The **LC_p** simulations were run keeping parameters of the simulation similar to the **fiducial** Quijote run, except for f_{NL} which was set to 100. The true f_{NL} is within 1σ , and the $\delta_m + \pi$ constraints are again 2.2 times better than the $\delta_m + \delta_h$ based analysis, consistent with the improvement in the Gaussian case.

When we extend our analysis to 100 simulations for

$f_{NL} = 0$, we find a small ($\Delta f_{NL} \sim 8$) additive bias, which goes away if we decrease k_{\max} from its fiducial value ($0.047 h^{-1}\text{Mpc}$). We interpret it as arising from breakdown of the linear bias model ($\pi = b_\pi \delta_m + \text{noise}$) on small scales. For a single simulation volume ($1 (\text{Gpc}/h)^3$) the bias is small. For a larger survey volume, the bias would need to be addressed, either by decreasing k_{\max} , or by including more terms in the bias model.

So far, we have chosen to use five matter-derived π -fields $\{\pi_i^m\}_{1 \leq i \leq 5}$, corresponding to different small-scale k -bins (see §IV B). We next explore the impact of varying these choices.

As explained in II, defining and using multiple π^m fields over a k_s window provides more information than using a single π^m field over the same k_s window. Instead of using five π_i^m fields covering the range $0.5 \leq k_s \leq 3.0$, we tried using a single π_{coarse}^m field defined over the same k_s -range. We find that the single-simulation f_{NL} constraint degrades significantly, from $\sigma(f_{NL}) \sim 25$ to $\sigma(f_{NL}) \sim 37$.

Finally, to demonstrate how sensitivity to f_{NL} increases as we go deeper into the non-linear regime, in Fig. 4, we look at how the constraint $\sigma(f_{NL})$ on f_{NL} evolves as a function of k in our analysis by combining δ_m with π fields which have their k -filter centered at increasingly non-linear scales. As can be seen, the constraints improve monotonically as more and more π fields are included in the analysis, suggesting the presence of f_{NL} sensitive information in the highly non-linear regime. We note that there appears to be almost no extra information contained in the highest k bin, even though Fig. 1 shows that the noise in this bin is very low. This means that this bin is highly correlated with the lower k bins. Physically this may be because we have entered the 1-halo regime, but we have not investigated this question in detail.

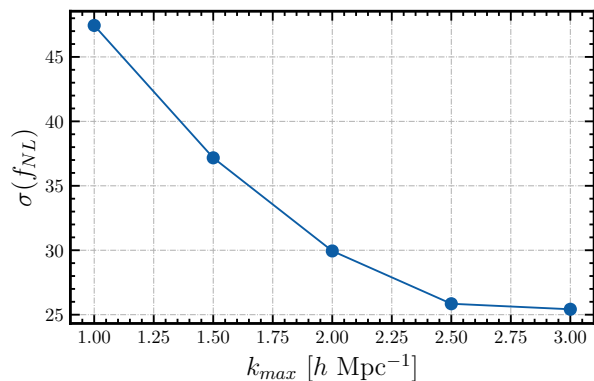


Figure 4. Constraints on f_{NL} as a function of k_{\max} , the largest wavenumber where the matter field $\delta_m(\mathbf{k})$ is observed. We increase k_{\max} by adding the fields $\{\pi_i^m\}_{1 \leq i \leq 5}$ (defined in §IV B) one at a time to our MCMC analysis. The reported sensitivity is for a simulation volume of $1 (h^{-1}\text{Gpc})^3$.

B. Halo field based results from Quijote

In the previous section, we assumed that the matter field was observable on small scales. In this section, we (more realistically) assume that the small-scale halo field is observed and used to construct the π field. We will present two slightly different versions of the analysis, with and without the large-scale matter field, in Figs. 6 and 7 below.

First we constrain f_{NL} using large-scale power spectra of the fields δ_m , δ_h , and π_i^h (we will drop δ_m below). Here, the fields $\{\pi_i^h\}_{i=1,2}$ were defined in §IV B, and correspond to locally measured small-scale halo power in a certain k -range (k_{\min}^i, k_{\max}^i).

In Fig. 5, we show the large-scale bias of the π_i^h -fields:

$$b_{\pi_i^h}^G(k) = \frac{P_{m\pi_i^h}(k)}{P_{mm}(k)} \quad (35)$$

and compare it to halo bias b_h^G . As can be seen, the π_i^h -bias starts deviating from a scale-independent constant value starting at $k \sim 0.015 h^{-1}\text{Mpc}$. Therefore we conclude that our linear bias for the π_i^h fields is valid below this scale, and restrict the MCMC to $k_{\max} = 0.0125 h^{-1}\text{Mpc}$, corresponding to the largest 20 modes of the simulation volume.

In the left panel of Fig. 6, we present marginalized constraints on f_{NL} from our analysis of $\delta_m + \delta_h$ and compare it to the constraints obtained from $\delta_m + \delta_h + \pi_i^h$. We find that by adding the π_i^h fields to the MCMC analysis, we obtain negligible improvement in our uncertainty on f_{NL} . In the right panel of Fig. 6, we present results of an identical analysis but for simulations with $f_{NL} = 100$, showing that the correct value of f_{NL} is recovered (within statistical errors).

So far, we have assumed that the matter field is observed on large scales (but not small scales), and the halo field is observed on all scales. In Fig. 7, we eliminate the matter field from the analysis, and continue to assume that the halo field is observed on all scales. The first curve (labelled δ_h) uses the power spectrum P_{hh} on large scales. The second curve (labelled $\delta_h + \pi_i^h$) uses large-scale power spectra of the form P_{hh} , $P_{h\pi_i^h}$, and $P_{\pi_i^h\pi_j^h}$. In N -point language, this analysis includes the squeezed trispectrum B_{hhh} and collapsed trispectrum T_{hhhh} .

Due to the limited number of modes being used, we find that it's not possible to constrain all the bias and noise parameters simultaneously with the f_{NL} parameter. We therefore decide to fix the noise parameters to their values obtained from the $\delta_m + \delta_h + \pi_i^h$ analysis described above. After fixing the noise parameters in our MCMC pipeline, we run it to obtain constraints on the bias and f_{NL} and present the marginalized constraint on f_{NL} . We find that in this analysis without the matter field, the relative improvement in $\sigma(f_{NL})$ from adding π_i^h -fields is non-negligible, but still small. We obtain $\sim 25\%$ improvement in the marginalized error bound. In both cases, we don't observe any systematic bias in

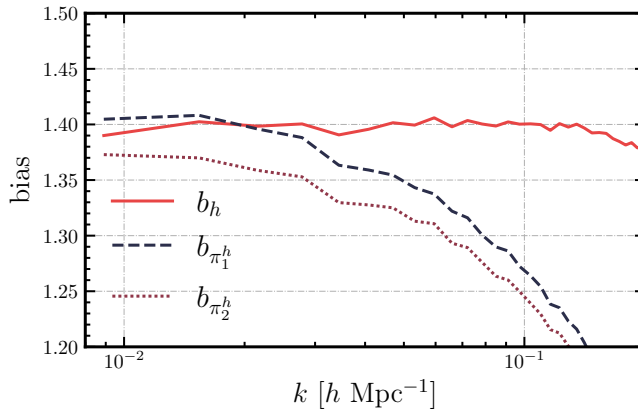


Figure 5. Bias measured in $f_{NL} = 0$ simulations for the two halo-derived π fields $\{\pi_i^h\}_{1 \leq i \leq 2}$ defined in IV B, and for the halo field δ_h . The curves demonstrate that unlike halo bias b_h which remains constant even at $k = 0.1 h^{-1} \text{Mpc}$, the bias of π_i^h starts deviating from a constant at $k \sim 0.015 h^{-1} \text{Mpc}$. We use this result as a justification for truncating the MCMC likelihood in our halo-based analysis (§V B) at $k_{max} = 0.0125 h^{-1} \text{Mpc}$, corresponding to the 20 largest modes in the simulation volume.

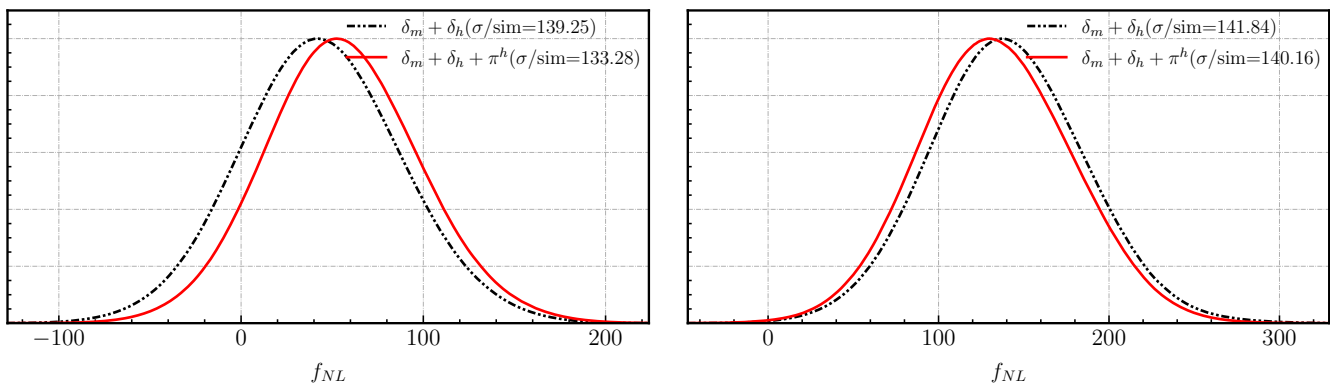


Figure 6. *Left.* MCMC constraints on f_{NL} from $\delta_m + \delta_h$, compared to constraints from $\delta_m + \delta_h + \pi_i^h$, where π_i^h denotes the halo-derived π -fields π_1^h and π_2^h defined in IV B. The two π_i^h fields correspond intuitively to locally measured small-scale halo power in two different k_S -bins. *Right.* Constraints on f_{NL} for $f_{NL} = 100$ simulations. In both these cases we use 10 Quijote simulations (same set as that used in Fig. 3) with likelihood truncated at $k = 0.0125 h \text{Mpc}^{-1}$ corresponding to the largest 20 modes in the simulation volume. The improvement in $\sigma(f_{NL})$ from adding the π_i^h fields is marginal.

the recovered f_{NL} estimate.

Summarizing, in this section we compared a “standard” analysis of large-scale δ_m and δ_h fields to an “extended” analysis which also includes π_i^h -fields. Our main result is that the improvement in $\sigma(f_{NL})$ is marginal.

In this analysis, we have used $k_{max} = 0.0125 h^{-1} \text{Mpc}$, since the π_i^h -bias in Fig. 5 is only constant on the largest scales. It is possible that by using a higher order bias model, one could include smaller scales. It seems unlikely to us that increasing k_{max} would change our results qualitatively, for the following reason. In Figs. 6, 7, the standard and extended analyses use the same value of k_{max} . If k_{max} is increased consistently in both analyses, then both values of $\sigma(f_{NL})$ will decrease, but it seems unlikely that the ratio of $\sigma(f_{NL})$ values (or f_{NL} information per mode) would change.

C. Comparison with previous work

In this section, we compare our results with related work (described in the introduction) by Goldstein et. al. [36] and the Quijote-PNG collaboration [29–32].

The analysis in [36] uses the squeezed ($k_L \ll k_S$) matter bispectrum over the following scales (units h/Mpc):

$$0.005 < k_L < 0.06 \quad 0.2 < k_S < 0.6 \quad (36)$$

and finds statistical error $\sigma(f_{NL}) = 12$ at $z = 0$ for simulation volume $(2.4 \text{ Gpc}/h)^3$. Scaling this to the Quijote volume $(1 \text{ Gpc}/h)^3$, assuming $\sigma(f_{NL}) \propto V^{-1/2}$, gives $\sigma(f_{NL}) = 45$.

This can be compared to our $(\delta_m + \pi_i^m)$ analysis from §V A, which gives $\sigma(f_{NL}) = 25$, a factor 1.8 better. There are two major differences between our analysis and [36] which may be responsible for the different $\sigma(f_{NL})$. First,

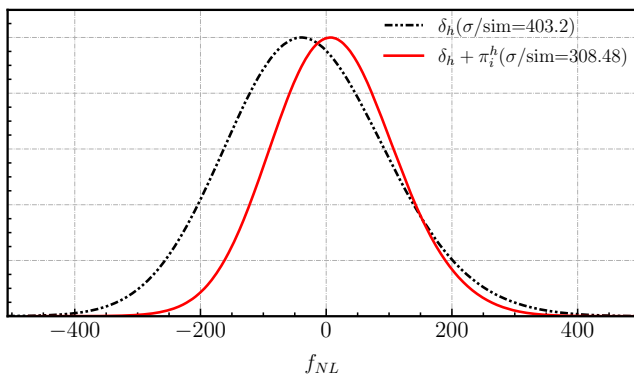


Figure 7. MCMC constraints on f_{NL} from δ_h compared to constraints from $\delta_h + \pi_i^h$, where π_i^h denotes the halo-derived π -fields $\{\pi_i^h\}_{i=1,2}$ defined in IV B. The two π_i^h fields correspond intuitively to locally measured small-scale halo power in two different k_S -bins. The analysis uses 10 Quijote simulations with Gaussian initial conditions (same set as that used in Fig. 3) with likelihood truncated at $k = 0.012 h^{-1}\text{Mpc}$. The noise $N_{\pi_i\pi_j}$ is fixed to the values obtained from $\delta_m + \delta_h + \pi^h$ analysis (Figure VB). The improvement in $\sigma(f_{NL})$ from adding the π_i^h fields is moderate but not negligible (about 25%).

we use a different range of scales:

$$0.006 < k_L < 0.047 \quad 0.5 < k_S < 3.0 \quad (37)$$

in the same notation as Eq. 36. Second, our $(\delta_m + \pi_i^m)$ analysis includes collapsed trispectrum information, in addition to squeezed bispectrum information.

Next, we compare our results to the Quijote-PNG [29–32] analysis of local-type non-Gaussianity. (The Quijote-PNG papers also analyze equilateral and orthogonal-type non-Gaussianity, but this is outside the scope of this paper.) The two analyses are closely related: we study the same high-level questions and use the same simulation parameters. However, the details are very different as follows.

First, the two analyses use N -point functions on different scales. The Quijote-PNG analysis uses two-point and three-point functions with $k_{\max} = 0.5$ (units $h \text{ Mpc}^{-1}$ throughout). In contrast, we use the two-point function on large scales ($k \lesssim 0.05$), the 3-point function in “squeezed” configurations (Eq. (37)), and the 4-point function in “collapsed” configurations

$$|\mathbf{k}_1 + \mathbf{k}_2| \lesssim 0.05 \quad 0.5 \lesssim \{k_1, k_2, k_3, k_4\} \lesssim 3.0 \quad (38)$$

Thus, the two analyses are highly complementary. For the 2-point function, our analysis contains less information (lower k_{\max}) than Quijote-PNG. For the 3-point function, neither analysis is a subset of the other. Finally, our analysis includes some 4-point information, whereas Quijote-PNG does not use the 4-point function. (We note that since the two analyses are so complementary, it should be possible to combine them in an analysis to tighten f_{NL} constraints further.)

Second, the Quijote-PNG analysis marginalizes ΛCDM cosmological parameters (and for analyses including halos, a minimum halo mass M_{\min}), but does not marginalize a complete set of astrophysical nuisance parameters at $k_{\max} = 0.05$ (e.g. EFT coefficients, higher-order halo biases).

In contrast, we have argued that by marginalizing bias and noise parameters b_π , $N_{\pi\pi'}$, we automatically marginalize over all nuisance parameters in sight (cosmological or astrophysical). This is because primordial non-Gaussianity produces signals with a distinctive $1/k^2$ scale dependence.

Finally, the details of the forecasting procedure are quite different (MCMC versus Fisher), and in particular we do not need a large suite of N -body simulations in order to estimate covariances and cosmological parameter derivatives.

Despite these differences, our conclusions are very similar to Quijote-PNG. If the matter field can be observed on small scales, then strong f_{NL} constraints can be obtained. Quijote-PNG finds $\sigma(f_{NL}) \sim 35$ at $z = 0^4$, whereas we find $\sigma(f_{NL}) = 25$, a factor 1.4 better. As with our comparison with [36] above, the improvement could be due either to the different scales in the two analyses, or to our inclusion of four-point information.

On the other hand, if we only have observations of the small-scale halo field, then improvements from using higher N -point functions are marginal (compared to a two-point analysis). We are surprised by the level of agreement with Quijote-PNG, since the analyses are so different (see above), and so we expect that these conclusions are quite robust.

VI. CONCLUSION

In this work, we have presented a simulation based approach for constraining local primordial non-Gaussianity parameter f_{NL} from current and upcoming galaxy survey datasets. The approach involves computing auxiliary fields π using small-scale modes of galaxy or halo fields. The π -fields are quadratic in δ_g or δ_h and intuitively correspond to locally measured small-scale power. These fields “encode” higher-point information, in the sense that large-scale power spectra ($P_{m\pi}$ or $P_{\pi\pi}$) are equivalent to higher N -point functions (squeezed bispectrum or collapsed trispectrum).

We have validated our formalism and developed an end-to-end MCMC pipeline to test the constraining power of the approach when applied to matter and halo fields obtained from N -body simulations. The main idea

⁴ We read off the value $\sigma(f_{NL}) \sim 35$ from Fig. 6 of [29], right column, curve labelled “Local” and “Marg. ΛCDM params”.

is that on large scales, the π -fields can be modelled as:

$$\pi(\mathbf{k}) = \left(b_\pi + 2\beta_\pi \frac{f_{NL}}{\alpha(k, z)} \right) \delta_m(\mathbf{k}) + (\text{Gaussian noise}) \quad (39)$$

This simple-looking statement turns out to have several very interesting consequences.

The Gaussianity of the noise means that we can analyze higher N -point functions in a simple way by sampling a Gaussian likelihood function (35) for the large-scale modes of the δ_m and π fields. Although the likelihood is Gaussian, it incorporates (via sample variance of the π -fields) nontrivial higher-point contributions to the bispectrum and trispectrum covariance. We have tested Gaussianity of the noise in Fig. 2.

The simplicity of the bias model (39) means that our approach requires minimal modelling. In fact, in a Gaussian ($f_{NL} = 0$) cosmology there is no modelling at all – we simply treat b_π and $N_{\pi\pi'}$ as free parameters, to be marginalized in our MCMC sampler. This procedure automatically marginalizes uncertainty in cosmological and astrophysical nuisance parameters, regardless of the details of these parameters. This is because the $1/k^2$ scaling in (39) in an $f_{NL} \neq 0$ universe is robust to small-scale peculiarities like aliasing and resolution effects as well as poorly understood baryonic physics. We have tested the bias model (39) directly in Figs. 1, 5. Additionally, we have done “end-to-end” tests of our analysis, by verifying that we recover unbiased f_{NL} values in simulations (Figs. 3, 6, 7).

One final advantage of our approach is that it is straightforward to include other large-scale tracer fields. For example, we could seamlessly include reconstructed kSZ velocity [52, 54] for sample variance cancellation.

Remarkably, we find that this simple, low computational cost procedure gives results which are qualitatively consistent with previous studies [29–32, 36]. In fact, if the matter field can be directly observed on small scales, then our $\sigma(f_{NL})$ is a little better than values reported in these studies (see §V C). This could be either because our procedure includes collapsed 4-point information, or because we can use deeply nonlinear modes at very high k . Indeed, because we do not need to model these scales in detail, we can extract f_{NL} sensitive information from extremely non-linear scales approaching k_{nyquist} . In practice, we find that as k_{max} is increased, $\sigma(f_{NL})$ decreases slowly and eventually saturates (Fig. 4).

There is one type of parameter which we do need to model: non-Gaussian biases β_h , β_π . This is an issue for essentially all proposals for constraining f_{NL} from large-scale structure, including non-Gaussian halo bias [55, 56], and the discussion below applies generally. In the simulation-based approach of this paper, we assume per-

fect knowledge of non-Gaussian biases β_h and β_π , which we compute following Eq. 31. However, in a more realistic setup, these parameters are not known in advance, and would need to be modelled somehow. For example, we could use N -body simulations (with astrophysical parameters varied over some reasonable range), perturbation theory, or the halo model. In practice, non-Gaussian biases are degenerate with f_{NL} (they always appear in the combination $\beta_\pi f_{NL}$), and so incorrect modelling of β_π cannot “fake” a detection of nonzero f_{NL} (only the f_{NL} normalization). For this reason, we have de-emphasized the issue in this initial study.

When we apply our methods to the halo field δ_h , instead of assuming the matter field δ_m is directly measurable, we find only marginal improvements (§V B). The squeezed halo bispectrum B_{hhh} and collapsed halo trispectrum T_{hhhh} add little f_{NL} information to the halo power spectrum P_{hh} . Similar results were found by the Quijote-PNG collaboration [29–32] using very different assumptions and methods. However, both studies use the Quijote simulations, where the mass resolution is modest. It seems plausible to us that higher N -point functions may be more useful at higher mass resolution, where halo number densities are larger. In a future study, we plan to explore f_{NL} sensitivity for a higher tracer density sample from simulations like AbacusSummit [57, 58].

ACKNOWLEDGEMENTS

We thank William Coulton, Sam Goldstein, Oliver Philcox and Francisco Villaescusa-Navarro for useful comments on the manuscript. Part of this work was performed at the Aspen Center for Physics, which is supported by National Science Foundation grant PHY-1607611. MM acknowledges support from DOE grant DE-SC0022342. Support for this research was provided by the University of Wisconsin - Madison Office of the Vice Chancellor for Research and Graduate Education with funding from the Wisconsin Alumni Research Foundation. KMS was supported by an NSERC Discovery Grant and a CIFAR fellowship. Research at Perimeter Institute is supported in part by the Government of Canada through the Department of Innovation, Science and Economic Development Canada and by the Province of Ontario through the Ministry of Colleges and Universities. Perimeter Institute’s HPC system “Symmetry” was used to perform some of the analysis presented in the letter. We have extensively used several python libraries including NUMPY[59], MATPLOTLIB[60], CLASS[61], GET-DIST[62] and SCIENCEPLOTS[63].

[1] A. Aghamousa *et al.*, arXiv preprint arXiv: Arxiv-1611.00036 (2016).

[2] R. Laureijs *et al.*, arXiv preprint arXiv: Arxiv-1110.3193 (2011).

- [3] P. A. Abell *et al.* (LSST Science, LSST Project), (2009), arXiv:0912.0201 [astro-ph.IM].
- [4] X. Chen, arXiv preprint arXiv: Arxiv-1002.1416 (2010).
- [5] A. Achúcarro *et al.*, (2022), arXiv:2203.08128 [astro-ph.CO].
- [6] N. Aghanim *et al.* (Planck), *Astron. Astrophys.* **641**, A6 (2020), [Erratum: *Astron. Astrophys.* 652, C4 (2021)], arXiv:1807.06209 [astro-ph.CO].
- [7] M. Alvarez *et al.*, (2014), arXiv:1412.4671 [astro-ph.CO].
- [8] N. Dalal, O. Dore, D. Huterer, and A. Shirokov, *Phys. Rev. D* **77**, 123514 (2008), arXiv:0710.4560 [astro-ph].
- [9] A. Slosar, C. Hirata, U. Seljak, S. Ho, and N. Padmanabhan, *Journal of Cosmology and Astroparticle Physics* **2008** (08), 031.
- [10] M. Biagetti, *Galaxies* **7**, 71 (2019).
- [11] N. Sailer, E. Castorina, S. Ferraro, and M. White, *JCAP* **12** (12), 049, arXiv:2106.09713 [astro-ph.CO].
- [12] A. Andrews, J. Jasche, G. Lavaux, and F. Schmidt, *Mon. Not. Roy. Astron. Soc.* **520**, 5746 (2023), arXiv:2203.08838 [astro-ph.CO].
- [13] O. Friedrich, C. Uhlemann, F. Villaescusa-Navarro, T. Baldauf, M. Manera, and T. Nishimichi, *Mon. Not. Roy. Astron. Soc.* **498**, 464 (2020), arXiv:1912.06621 [astro-ph.CO].
- [14] M. Biagetti, A. Cole, and G. Shiu, *JCAP* **04**, 061, arXiv:2009.04819 [astro-ph.CO].
- [15] U. Giri, M. Münchmeyer, and K. M. Smith, *Phys. Rev. D* **107**, L061301 (2023).
- [16] D. Jeong and E. Komatsu, *The Astrophysical Journal* **703**, 1230–1248 (2009), arXiv:0904.0497.
- [17] T. Baldauf, U. Seljak, and L. Senatore, *Journal of Cosmology and Astroparticle Physics* **2011** (04), 006–006, arXiv:1011.1513.
- [18] M. Schmittfull, T. Baldauf, and U. Seljak, *Physical Review D* **91**, 10.1103/physrevd.91.043530 (2015), arXiv:1411.6595.
- [19] C.-T. Chiang, *Physical Review D* **95**, 10.1103/physrevd.95.123517 (2017), arXiv:1701.03374.
- [20] R. de Putter, *Primordial physics from large-scale structure beyond the power spectrum* (2018), arXiv:1802.06762.
- [21] A. M. Dizgah, H. Lee, M. Schmittfull, and C. Dvorkin, *Journal of Cosmology and Astroparticle Physics* **2020** (04), 011–011, arXiv:1911.05763.
- [22] J.-P. Dai, L. Verde, and J.-Q. Xia, *Journal of Cosmology and Astroparticle Physics* **2020** (08), 007–007, arXiv:2002.09904.
- [23] O. Darwish, S. Foreman, M. M. Abidi, T. Baldauf, B. D. Sherwin, and P. D. Meerburg, *Density reconstruction from biased tracers and its application to primordial non-gaussianity* (2020), arXiv:2007.08472.
- [24] A. Moradinezhad Dizgah, M. Biagetti, E. Sefusatti, V. Desjacques, and J. Noreña, *JCAP* **05**, 015, arXiv:2010.14523 [astro-ph.CO].
- [25] G. Cabass, M. M. Ivanov, O. H. E. Philcox, M. Simonović, and M. Zaldarriaga, *Phys. Rev. D* **106**, 043506 (2022), arXiv:2204.01781 [astro-ph.CO].
- [26] G. D’Amico, M. Lewandowski, L. Senatore, and P. Zhang, (2022), arXiv:2201.11518 [astro-ph.CO].
- [27] A. Barreira, *JCAP* **03**, 008, arXiv:1901.01243 [astro-ph.CO].
- [28] T. Flöss, M. Biagetti, and P. D. Meerburg, *Phys. Rev. D* **107**, 023528 (2023), arXiv:2206.10458 [astro-ph.CO].
- [29] W. R. Coulton, F. Villaescusa-Navarro, D. Jamieson, M. Baldi, G. Jung, D. Karagiannis, M. Liguori, L. Verde, and B. D. Wandelt, *Quijote-png: Simulations of primordial non-gaussianity and the information content of the matter field power spectrum and bispectrum* (2022).
- [30] G. Jung, D. Karagiannis, M. Liguori, M. Baldi, W. R. Coulton, D. Jamieson, L. Verde, F. Villaescusa-Navarro, and B. D. Wandelt, *Quijote-png: Quasi-maximum likelihood estimation of primordial non-gaussianity in the non-linear dark matter density field* (2022).
- [31] W. R. Coulton, F. Villaescusa-Navarro, D. Jamieson, M. Baldi, G. Jung, D. Karagiannis, M. Liguori, L. Verde, and B. D. Wandelt, *Quijote png: The information content of the halo power spectrum and bispectrum* (2022).
- [32] G. Jung, D. Karagiannis, M. Liguori, M. Baldi, W. R. Coulton, D. Jamieson, L. Verde, F. Villaescusa-Navarro, and B. D. Wandelt, arXiv preprint arXiv: Arxiv-2211.07565 (2022).
- [33] R. E. Angulo and O. Hahn 10.1007/s41115-021-00013-z (2021), arXiv:2112.05165 [astro-ph.CO].
- [34] N. E. Chisari, A. Mead, S. Joudaki, P. Ferreira, A. Schneider, J. Mohr, T. Tröster, D. Alonso, I. McCarthy, S. Martin-Alvarez, J. Devriendt, A. Slyz, and M. van Daalen, *The Open Journal Of Astrophysics* 10.21105/astro.1905.06082 (2019).
- [35] F. Villaescusa-Navarro *et al.*, *Astrophys. J.* **915**, 71 (2021), arXiv:2010.00619 [astro-ph.CO].
- [36] S. Goldstein, A. Esposito, O. H. E. Philcox, L. Hui, J. C. Hill, R. Scoccimarro, and M. H. Abitbol, *Phys. Rev. D* **106**, 123525 (2022), arXiv:2209.06228 [astro-ph.CO].
- [37] M. Peloso and M. Pietroni, *JCAP* **05**, 031, arXiv:1302.0223 [astro-ph.CO].
- [38] A. Kehagias and A. Riotto, *Nucl. Phys. B* **873**, 514 (2013), arXiv:1302.0130 [astro-ph.CO].
- [39] M. Simonovic, *Cosmological Consistency Relations*, Ph.D. thesis, SISSA, Trieste (2014).
- [40] C.-T. Chiang, C. Wagner, F. Schmidt, and E. Komatsu, *JCAP* **05**, 048, arXiv:1403.3411 [astro-ph.CO].
- [41] F. Villaescusa-Navarro *et al.*, *Astrophys. J. Suppl.* **250**, 2 (2020), arXiv:1909.05273 [astro-ph.CO].
- [42] S. Cheng, Y.-S. Ting, B. Ménard, and J. Bruna, *Monthly Notices of the Royal Astronomical Society* **499**, 5902–5914 (2020), arXiv:2006.08561.
- [43] J. M. Sullivan, T. Prijon, and U. Seljak, (2023), arXiv:2303.08901 [astro-ph.CO].
- [44] V. Desjacques, U. Seljak, and I. Iliev, *Mon. Not. Roy. Astron. Soc.* **396**, 85 (2009), arXiv:0811.2748 [astro-ph].
- [45] M. Biagetti, T. Lazeyras, T. Baldauf, V. Desjacques, and F. Schmidt, *Monthly Notices of the Royal Astronomical Society* **468**, 3277 (2017).
- [46] V. Springel, *Mon. Not. Roy. Astron. Soc.* **364**, 1105 (2005), arXiv:astro-ph/0505010.
- [47] M. Crocce, S. Pueblas, and R. Scoccimarro, *Mon. Not. Roy. Astron. Soc.* **373**, 369 (2006), arXiv:astro-ph/0606505.
- [48] M. Davis, G. Efstathiou, C. S. Frenk, and S. D. M. White, *Astrophys. J.* **292**, 371 (1985).
- [49] F. Villaescusa-Navarro, *Pylians: Python libraries for the analysis of numerical simulations*, *Astrophysics Source Code Library*, record ascl:1811.008 (2018), ascl:1811.008.
- [50] R. W. Hockney and J. W. Eastwood, *Computer simulation using particles* (1988).
- [51] N. Hand, Y. Feng, F. Beutler, Y. Li, C. Modi, U. Seljak, and Z. Slepian, *Astron. J.* **156**, 160 (2018),

- arXiv:1712.05834 [astro-ph.IM].
- [52] U. Giri and K. M. Smith, *Journal of Cosmology and Astroparticle Physics* **2022** (09), 028.
- [53] D. Foreman-Mackey, D. W. Hogg, D. Lang, and J. Goodman, *PASP* **125**, 306 (2013), 1202.3665.
- [54] M. Münchmeyer, M. S. Madhavacheril, S. Ferraro, M. C. Johnson, and K. M. Smith, *Phys. Rev. D* **100**, 083508 (2019), arXiv:1810.13424 [astro-ph.CO].
- [55] A. Barreira, *JCAP* **11**, 013, arXiv:2205.05673 [astro-ph.CO].
- [56] A. Barreira, *JCAP* **01** (01), 033, arXiv:2107.06887 [astro-ph.CO].
- [57] N. A. Maksimova, L. H. Garrison, D. J. Eisenstein, B. Hadzhiyska, S. Bose, and T. P. Satterthwaite, *Monthly Notices of the Royal Astronomical Society* **508**, 4017 (2021), <https://academic.oup.com/mnras/article-pdf/508/3/4017/40811763/stab2484.pdf>.
- [58] L. H. Garrison, D. J. Eisenstein, D. Ferrer, N. A. Maksimova, and P. A. Pinto, *Monthly Notices of the Royal Astronomical Society* **508**, 575 (2021), <https://academic.oup.com/mnras/article-pdf/508/1/575/40458823/stab2482.pdf>.
- [59] C. R. Harris *et al.*, *Nature* **585**, 357 (2020).
- [60] J. D. Hunter, *Computing in Science & Engineering* **9**, 90 (2007).
- [61] D. Blas, J. Lesgourgues, and T. Tram, *Journal of Cosmology and Astroparticle Physics* **2011** (07), 034.
- [62] A. Lewis, (2019), arXiv:1910.13970 [astro-ph.IM].
- [63] J. D. Garrett 10.5281/zenodo.4106649 (2021).